

General Application of Numerical Green's Functions for SIF Computations With Boundary Elements

S. Guimarães¹ and J.C.F. Telles²

Abstract: The paper discusses further applications of the hyper-singular boundary integral equation to obtain the Green's function solution to general geometry fracture mechanics problems, such as curved multifracture crack simulation, static and transient dynamic in 2-D, 3-D and plate bending problems. This numerical Green's function (NGF) is implemented into alternative boundary element computer programs, as the fundamental solution, to enhance the scope of alternative applications of the NGF procedure.

The results to some typical linear fracture mechanics problems are presented.

keyword: HBEM, Crack, Green's Function

1 Introduction

It is widely known that the appropriate numerical modelling of linear elastic fracture mechanics problems strongly depends on the stress field accuracy in the vicinity of the crack tip. Usually this is achieved by a good mesh refinement associated to the usage of special tip elements when the numerical computation is performed. With regard to the BEM, however, another difficulty arises; the crack surfaces geometrically coincide in the numerical model causing a degeneration of the boundary integral equation. This problem is usually avoided by:

- Modeling the crack as a narrow elliptic cavity;
- Considering symmetry, whenever possible;
- Applying the sub-region technique (Blandford, Ingraffea, and Liggett, 1981)
- Employing the mixed or dual formulation (Cruse, 1975; Portela, Aliabadi, and Rooke, 1992; Guimarães and Telles, 1994);
- Using the associated Green's function (Snyder and Cruse, 1975).

The last three procedures above are the most important and widely used techniques in BEM to solve LEFM problems. The difference between these three approaches is illustrated as follows. The integral equations necessary to solve crack prob-

¹ Faculdade de Engenharia/UERJ, Dpto Engenharia Mecânica, Rio de Janeiro, Brazil

² COPPE/UFRJ, Programa de Engenharia Civil, Rio de Janeiro, Brazil

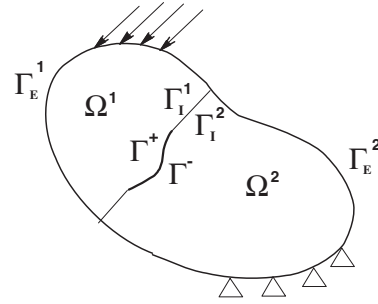


Figure 1 : Sub-region Formulation Model

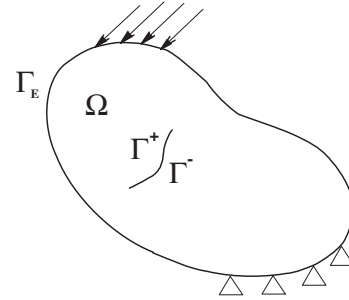


Figure 2 : Mixed or Dual Formulation Model

lems by the subregion technique, Figure 1, are (superscript * represents fundamental solution, e.g. Kelvin):

$$C_{ij}(\xi)u_j(\xi) = \int_{\Gamma_E^1 + \Gamma_I^1 + \Gamma^+} u_{ij}^*(\xi, x) p_j(x) d\Gamma(x) - \int_{\Gamma_E^2 + \Gamma_I^2 + \Gamma^+} p_{ij}^*(\xi, x) u_j(x) d\Gamma(x) \quad \xi \in (\Gamma_E^1 \cup \Gamma_I^1 \cup \Gamma^+) \quad (1)$$

$$C_{ij}(\xi)u_j(\xi) = \int_{\Gamma_E^2 + \Gamma_I^2 + \Gamma^-} u_{ij}^*(\xi, x) p_j(x) d\Gamma(x) - \int_{\Gamma_E^1 + \Gamma_I^1 + \Gamma^-} p_{ij}^*(\xi, x) u_j(x) d\Gamma(x) \quad \xi \in (\Gamma_E^2 \cup \Gamma_I^2 \cup \Gamma^-) \quad (2)$$

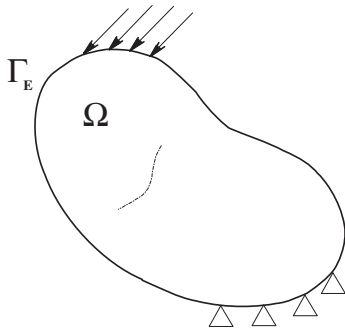


Figure 3 : Fundamental Green's Function Model.

where ξ is the source point and x , the field point. Problem displacements are denoted by u_j and tractions by p_j .

The equations (classical and hyper-singular) used to solve the same kind of problem by the mixed or dual formulation, shown in Figure 2, are:

$$C_{ij}(\xi)u_j(\xi) = \int_{\Gamma_E+\Gamma^++\Gamma^-} u_{ij}^*(\xi, x) p_j(x) d\Gamma(x) - \int_{\Gamma_E+\Gamma^++\Gamma^-} p_{ij}^*(\xi, x) u_j(x) d\Gamma(x) \quad \xi \in \Gamma_E \tag{3}$$

$$\frac{u_i(\xi^+)}{2} + \frac{u_i(\xi^-)}{2} = \int_{\Gamma_E+\Gamma^++\Gamma^-} u_{ij}^*(\xi^+, x) p_j(x) d\Gamma(x) - \int_{\Gamma_E+\Gamma^++\Gamma^-} p_{ij}^*(\xi^+, x) u_j(x) d\Gamma(x) \tag{4}$$

$$\frac{p_i(\xi^-)}{2} - \frac{p_i(\xi^+)}{2} = \int_{\Gamma_E+\Gamma^++\Gamma^-} U_{ij}^*(\xi^-, x) p_j(x) d\Gamma(x) - \int_{\Gamma_E+\Gamma^++\Gamma^-} P_{ij}^*(\xi^-, x) u_j(x) d\Gamma(x) \tag{5}$$

where $\xi^+ \in \Gamma^+$ and $\xi^- \in \Gamma^-$. The starred capital letter kernels result from the application of the traction operator to the standard fundamental solution kernels.

The above integral description of the problem avoids the interface modelling scheme providing a smaller system of equations if compared to the sub-region technique.

An important alternative in treating fracture mechanics problems by the BEM is the implementation of a Green's function, that automatically includes the crack existence, as a fundamental solution (Snyder and Cruse, 1975). Crack modelling with

the associated Green's function is depicted in Figure 3. In this case, only the classic formulation is necessary to represent the model (the superscript G stands for the Green's function fundamental solution):

$$C_{ij}(\xi)u_j(\xi) = \int_{\Gamma_E} u_{ij}^G(\xi, x) p_j(x) d\Gamma(x) - \int_{\Gamma_E} p_{ij}^G(\xi, x) u_j(x) d\Gamma(x) + \underbrace{\int_{\Gamma^++\Gamma^-} u_{ij}^G(\xi, x) p_j(x) d\Gamma(x)}_{\text{zero or prescribed}} - \underbrace{\int_{\Gamma^++\Gamma^-} p_{ij}^G(\xi, x) u_j(x) d\Gamma(x)}_{\text{zero}}, \quad \xi \in \Gamma_E \tag{6}$$

The advantage of this formulation is the elimination of the crack surface unknown variable integration. With this approach typical difficulties in modelling LEFM problems by BEM are elegantly avoided.

The drawback of this approach is the restricted availability of Green's functions for general geometry or alternative problem definitions other than straight or circular arc 2-D static applications. As an alternative, the numerical computation of the associated Green's function of the fundamental problem (unit load applied in a multi-fractured infinite medium) can be achieved through the application of the traction formulation to compute the desired relative displacements (opening and sliding) of the crack surfaces (Telles, Castor, and Guimarães, 1995). This numerical Green's function (NGF) procedure has been proposed by the present authors in the recent past (Telles, Castor, and Guimarães, 1995; Barra and Telles, 1999; Silveira, Guimarães, and Telles, 1998; Castor and Telles, 1999). In 2-D, it has been observed (Telles, Castor, and Guimarães, 1994), that the NGF BEM procedure can be as accurate (in engineering terms) and faster than the analytical Green's function counterpart (Snyder and Cruse, 1975) in general applications. For 3-D, elastodynamics and plate bending, however, one does not have analytical Green's functions to compare efficiency, but the 2-D static case results clearly demonstrated that the procedure is competitive for practical problems.

The NGF procedure allows for the solution of the LEFM problems in two steps; after the numerical fundamental solution is obtained by solving the multi-fractured infinite medium problem, the BEM can be applied to solve the problem over the external boundary only (eqn(6)), leading to a smaller system of equations. Another feature of the strategy is the absence of standard boundary element crack discretization, especially useful when most of the cracks are small and of simple shape. The NGF approach is basically as easy to implement as the mixed (or dual) method, since both require computation of equivalent hyper-singular boundary integral equations, and

permits the addition of inclusions and other material defects into the fundamental solution.

A generalization of the NGF technique is introduced here, where 2-D curved, elastodynamic, plate bending and 3-D applications are discussed, including examples.

2 Numerical Fundamental Green's Function

As discussed in the first elastostatic applications (Telles, Castor, and Guimarães, 1995), the fundamental Green's function can be written in terms of a superposition of a full-space fundamental solution plus a complementary part which provides satisfaction of the traction free requirement over the crack surfaces. This Green's function can be represented by

$$u_{ij}^G(\xi, x) = u_{ij}^*(\xi, x) + u_{ij}^c(\xi, x) \quad (7)$$

$$p_{ij}^G(\xi, x) = p_{ij}^*(\xi, x) + p_{ij}^c(\xi, x) \quad (8)$$

where $u_{ij}^G(\xi, x)$ and $p_{ij}^G(\xi, x)$ are the fundamental displacement and traction, in j direction at the field point x due to a unit point load (with frequency ω , if dynamic) applied at the source point ξ in the i direction. The superscript $*$ stands for the full space standard fundamental solution (static or dynamic) and c indicates the complementary components of the fundamental problem.

Since $u_{ij}^*(\xi, x)$ and $p_{ij}^*(\xi, x)$ are known (Brebbia, Telles, and Wrobel, 1984), the complementary displacements and tractions, $u_{ij}^c(\xi, x)$ and $p_{ij}^c(\xi, x)$, are the unknowns of the problem. This solution can be written in terms of boundary integral equations as shown bellow (Telles, Castor, and Guimarães, 1995):

$$u_{ij}^c(\xi, x) = \int_{\Gamma^I} p_{jk}^*(x, \zeta) c_{ik}(\xi, \zeta) d\Gamma(\zeta) \quad (9)$$

$$p_{ij}^c(\xi, x) = \int_{\Gamma^I} P_{jk}^*(x, \zeta) c_{ik}(\xi, \zeta) d\Gamma(\zeta) \quad (10)$$

where $c_{ik}(\xi, \zeta) = u_{ik}^c(\xi, \zeta^S) - u_{ik}^c(\xi, \zeta^I)$ is the crack opening displacements of the Green's function in which S and I stand for "superior" and "inferior" surfaces of the crack ($\Gamma^F = \Gamma^S + \Gamma^I$). The sign of the integrals depends on the chosen surface of integration; in this case Γ^I has been adopted. The integral equation (10) is originated from the hyper-singular or traction formulation.

If the crack opening displacements are known, both equations (9) and (10) produce the complementary displacements and tractions at an internal point $x(x \in \Gamma^I)$, due to a unit point load at ξ . Hence, since the natural boundary condition of the complementary problem is prescribed and given by $p_{ij}^c(\xi, \zeta) = -p_{ij}^*(\xi, \zeta)$ over Γ^I , the limit of equation (10), as $x \rightarrow \Gamma^I$, produces a hyper-singular boundary integral equation for the desired fundamental relative crack displacements. This

limiting procedure yields as a final result

$$\oint_{\Gamma^I} P_{jk}^*(\bar{\zeta}, \zeta) c_{ik}(\xi, \zeta) d\Gamma(\zeta) = -p_{ij}^*(\xi, \bar{\zeta}) \quad (11)$$

where, the symbol \oint indicates Hadamard's finite part integral.

The integral equation (11) for $c_{ik}(\xi, \zeta)$ can be solved by any appropriate suitable method and once this fundamental opening displacements are known equations (9) and (10) are used to obtain the complementary part of the fundamental numerical Green's function of eqns (7) and (8). Hence, the final displacement integral equation (6) is now rewritten with the present notation:

$$\begin{aligned} C_{ij}(\xi) u_j(\xi) = & \int_{\Gamma^E} u_{ij}^G(\xi, x) p_j(x) d\Gamma(x) \\ & - \int_{\Gamma^E} p_{ij}^G(\xi, x) u_j(x) d\Gamma(x) \\ & + \int_{\Gamma^I} c_{ij}(\xi, x) p_j^S(x) d\Gamma(x) \quad \xi \in \Gamma^E \end{aligned} \quad (12)$$

where the last integral represents the crack loading contribution to the external boundary displacements, i. e. crack pressure, if it exists, taking into account that $p_j^I(x) = -p_j^S(x)$.

The real crack opening displacement of the problem can be obtained by a post-processing procedure, using the standard traction (hyper-singular) integral equation and employing the standard full space fundamental solution:

$$\begin{aligned} \oint_{\Gamma^I} P_{ij}^*(\xi, x) c_j(x) d\Gamma(x) = & \\ & - \int_{\Gamma^E} U_{ij}^*(\xi, x) p_j(x) d\Gamma(x) - p_i^S(\xi) \quad \xi \in \Gamma^E \end{aligned} \quad (13)$$

where $c_j(x)$ is the actual crack opening displacements.

3 Crack Opening Displacements Computation

This section presents the selected strategy adopted to compute the fundamental crack opening displacements of equation (11), i. e. , $c_{ik}(\xi, \zeta)$. In order to simplify the ideas and without loss of generality for 3-D and 2-D curved crack geometries, the particular case of a horizontal crack centred at the origin of the coordinate system will be discussed. Here, the components $P_{12}^*(\bar{\zeta}, \zeta)$ and $P_{21}^*(\bar{\zeta}, \zeta)$ of the full space hyper-singular solution are null, decoupling the system of equations into longitudinal and transversal crack opening displacement integrals:

$$\oint_{-a}^a P_{11}^*(\bar{\zeta}, \zeta) c_{i1}(\xi, \zeta) d\Gamma(\zeta) = -p_{i1}^*(\xi, \bar{\zeta}) \quad (14)$$

$$\oint_{-a}^a P_{22}^*(\bar{\zeta}, \zeta) c_{i2}(\xi, \zeta) d\Gamma(\zeta) = -p_{i2}^*(\xi, \bar{\zeta}) \quad (15)$$

where $2a$ is the crack size.

Notice that for static or dynamic applications, the singularities in the vicinity of $\bar{\zeta}$ are of the same order. Equations (14) and (15) can be solved by a standard weighted residual method, using the point collocation technique, to produce (manipulating only equation (14); the procedure for equation (15) is analogous):

$$\int_{-a}^a P_{11}^*(\bar{\zeta}_m, \zeta) c_{i1}(\xi, \zeta) d\Gamma(\zeta) = -p_{i1}^*(\xi, \bar{\zeta}_m); \quad m = 1, 2, \dots, M \quad (16)$$

Allowing for the occurrence of incorrections which can be separately rectified, the standard Gauss quadrature procedure can be employed in equation (16), in the following fashion:

$$|J| \sum_{n=1}^N \left(P_{11}^*(\bar{\zeta}_m, \zeta_n) c_{i1}(\xi, \zeta_n) W_n \right) - E_{i1} = -p_{i1}^*(\xi, \bar{\zeta}_m); \quad m = 1, 2, \dots, M \quad (17)$$

where $|J| = a$ is the Jacobian of the transformation to the intrinsic quadrature interval; ζ_n the corresponding point at the Gauss station n , W_n the associated weighting factor at this station and N the total number of integration points. The term E_{i1} is introduced to correct the result of the numerical integral so that the singularity associated differences between finite part and standard numerical integration are counterbalanced.

It is important to note that there is no need to interpolate formally $c_{i1}(\xi, \zeta_n)$ but simply compute its values at the Gauss points, later required for the regular integrals of equations (9) and (10).

In order to define E_{i1} , c_{i1} can be expanded in Taylor's series about the point $\bar{\zeta}_m$ to extract the singular terms of the integrand:

$$c_{ik}(\xi, \zeta) = c_{ik}(\xi, \bar{\zeta}_m) + \frac{\partial c_{ik}(\xi, \bar{\zeta}_m)}{\partial \Gamma(\zeta)} [\Gamma(\zeta) - \Gamma(\bar{\zeta}_m)] + \frac{1}{2} \frac{\partial^2 c_{ik}(\xi, \bar{\zeta}_m)}{\partial \Gamma(\zeta)^2} [\Gamma(\zeta) - \Gamma(\bar{\zeta}_m)]^2 + \dots \quad (18)$$

Equation (18) can be substituted in the integral of equation (16) to obtain the following:

$$\begin{aligned} \int_{-a}^a P_{11}^*(\bar{\zeta}_m, \zeta) c_{i1}(\xi, \zeta) d\Gamma(\zeta) = & \int_{-a}^a P_{11}^*(\bar{\zeta}_m, \zeta) c_{i1}(\xi, \bar{\zeta}_m) d\Gamma(\zeta) + \\ & \int_{-a}^a P_{11}^*(\bar{\zeta}_m, \zeta) \left\{ \frac{\partial c_{i1}(\xi, \bar{\zeta}_m)}{\partial \Gamma(\zeta)} [\Gamma(\zeta) - \Gamma(\bar{\zeta}_m)] \right\} d\Gamma(\zeta) + \\ & \int_{-a}^a P_{11}^*(\bar{\zeta}_m, \zeta) \left\{ \frac{1}{2} \frac{\partial^2 c_{i1}(\xi, \bar{\zeta}_m)}{\partial \Gamma(\zeta)^2} \right. \\ & \left. [\Gamma(\zeta) - \Gamma(\bar{\zeta}_m)]^2 + \dots \right\} d\Gamma(\zeta) \quad (19) \end{aligned}$$

The first two integrals on the right hand side of equation (19) have $O(r^{-2})$ and $O(r^{-1})$ integrands that generate a finite part and a Cauchy principal value integral, respectively. The last integral is regular and can be computed with a good numerical approximation by a Gauss integration technique. This last regular integral can be further simplified if one notice that from eqn (18):

$$\begin{aligned} \frac{1}{2} \frac{\partial^2 c_{ik}(\xi, \bar{\zeta}_m)}{\partial \Gamma(\zeta)^2} [\Gamma(\zeta) - \Gamma(\bar{\zeta}_m)]^2 + \dots = \\ c_{ik}(\xi, \zeta) - c_{ik}(\xi, \bar{\zeta}_m) - \frac{\partial c_{ik}(\xi, \bar{\zeta}_m)}{\partial \Gamma(\zeta)} [\Gamma(\zeta) - \Gamma(\bar{\zeta}_m)] \quad (20) \end{aligned}$$

Equation (20) provides simple means of defining the regular integrand of eqn(19). The other two singular integrals on the right of eqn (19) are to be computed using singular integration procedures, producing the final numerical system of equations (Telles, Castor, and Guimarães, 1995):

$$\begin{aligned} |J| \sum_{n=1}^N \left\{ P_{11}^*(\bar{\zeta}_m, \zeta_n) \left[c_{i1}(\xi, \zeta_n) - c_{i1}(\xi, \bar{\zeta}_m) \right. \right. \\ \left. \left. - \frac{\partial c_{i1}(\xi, \bar{\zeta}_m)}{\partial \Gamma(\zeta)} [\Gamma(\zeta_n) - \Gamma(\bar{\zeta}_m)] \right] W_n \right\} + \\ \int_{-a}^a P_{11}^*(\bar{\zeta}_m, \zeta) c_{i1}(\xi, \bar{\zeta}_m) d\Gamma(\zeta) + \\ \int_{-a}^a P_{11}^*(\bar{\zeta}_m, \zeta) \left\{ \frac{\partial c_{i1}(\xi, \bar{\zeta}_m)}{\partial \Gamma(\zeta)} [\Gamma(\zeta) - \Gamma(\bar{\zeta}_m)] \right\} d\Gamma(\zeta) = \\ - p_{i1}^*(\xi, \bar{\zeta}_m) ; \quad m = 1, 2, \dots, M \quad (21) \end{aligned}$$

Then, by comparing eqns (17) and (21), the correction term is defined as (Telles, Castor, and Guimarães, 1995) :

$$E_{i1}(\xi, \bar{\zeta}_m) = c_{i1}(\xi, \bar{\zeta}_m) e_{11}^{(1)} + \frac{\partial c_{i1}(\xi, \bar{\zeta}_m)}{\partial \Gamma(\zeta)} e_{11}^{(2)} \quad (22)$$

where

$$e_{11}^{(1)} = \sum_{n=1}^N P_{11}^*(\bar{\zeta}_m, \zeta_n) J_n W_n - \int_{-a}^a P_{11}^*(\bar{\zeta}_m, \zeta) d\Gamma(\zeta) \quad (23)$$

$$e_{11}^{(2)} = \sum_{n=1}^N P_{11}^*(\bar{\zeta}_m, \zeta_n) [\Gamma(\zeta_n) - \Gamma(\bar{\zeta}_m)] J_n W_n - \int_{-a}^a P_{11}^*(\bar{\zeta}_m, \zeta) [\Gamma(\zeta) - \Gamma(\bar{\zeta}_m)] d\Gamma(\zeta) \quad (24)$$

The correct finite part integrals, and principal values, of the singular terms can be calculated either analytically or using any existing appropriate numerical scheme. Furthermore, since the collocation points are taken to be the same as the Gauss integration ones (i.e., $M = N$), the crack opening derivatives at $\bar{\zeta}_m$ are needed. This is easily obtained by the adoption

of Lagrangean polynomial interpolations for $c_{ik}(\xi, \bar{\xi}_m)$ as explained elsewhere (Telles, Castor, and Guimarães, 1995).

The final equations, introducing also the results starting from equation (15), can be written in matrix form as

$$\left. \begin{matrix} S_1 c_{i1}(\xi) = p_{i1}(\xi) \\ S_2 c_{i2}(\xi) = p_{i2}(\xi) \end{matrix} \right\} \rightarrow S c_i(\xi) = p_i(\xi) \quad (25)$$

Matrices S_1 and S_2 are equal in 2-D static applications and different for dynamic applications. The decoupling of the equations system (25) into longitudinal and transversal crack "opening" displacements do not occur for the case of curved cracks but the approach is still the same.

It should be emphasized that matrix S is only a function of crack geometry. It remains the same for any position of the unit source point load. Hence, the system has to be solved just once, and subjected to back substitutions in a Gauss solution routine for other source points ξ . Therefore, the system matrix is independent of the external boundary shape and discretization. These facts make the implementation quite cost effective and competitive even in the case of simple crack geometries where a closed form Green's function may be available. Multiple cracks can be considered by letting the integrals over Γ^j , in the above expressions, be a sum of integrals over all crack boundaries: $\int_{\Gamma^j}(\dots) = \sum_{j=1}^J \int_{\Gamma_j^j}(\dots)$.

4 Special Implementation Features

4.1 2-D Curved Cracks

When the approach is implemented to curved cracks, the procedure described to produce the equation (21) is the same. The difficulty is in the evaluation of the correcting term containing the "analytic" finite part and principal values integrals, since there is no closed form integration formulae to apply. A regularization of the integral over the curved crack may be used as follows (Silveira, Guimarães, and Telles, 1998); consider the integration of the same singular integrand over a straight boundary $\gamma(\zeta')$ tangent to the curved boundary $\Gamma(\zeta)$ at the source point, $\bar{\xi}_m$. Allowing for changes of integration variables the following identity is valid:

$$\begin{aligned} \oint_{\Gamma} P_{jk}^*(\bar{\xi}_m, \zeta) d\Gamma(\zeta) = \\ \underbrace{\int_{-1}^1 \left[P_{jk}^*(\bar{\xi}_m, \zeta) \frac{\partial \Gamma(\zeta)}{\partial \eta} - P_{jk}^*(\bar{\xi}_m, \zeta') \frac{\partial \gamma(\zeta')}{\partial \eta} \right]}_{\text{regular}} d\eta + \\ \oint_{\gamma} P_{jk}^*(\bar{\xi}_m, \zeta') d\gamma(\zeta') \end{aligned} \quad (26)$$

The change of integration variables of the integrals over Γ and γ produce an equal free term for both transformations that cancel each other when the integrands are subtracted. Therefore,

only the integral over γ , whose analytical result is easily obtained (Telles, Castor, and Guimarães, 1995), is a finite part integral in eqn (26).

4.2 General 3-D

The difference is essentially the double integration associated with the crack surface representation which is more elaborate for singular integral computations.

The 3-D counterpart of eqn (26) reduces the order of the singular integrand, but does not produce a regular integral. Hence, polar coordinates and/or additional standard numerical schemes (Castor and Telles, 1999) are still recommended.

For quadrilateral crack surface geometry representation, the quadrangular surface element can be divided into triangular sub-elements, which are numerically integrated using polar coordinates, centred at the singular point. Hence, eqn(17) can be rewritten in the following form:

$$\begin{aligned} \sum_{\Delta} |G|_{\Delta} \left\{ \sum_{\theta} \sum_{\rho} |J|_{\theta\rho} \left(P_{jk}^*(\bar{\xi}_m, \zeta_{\theta\rho}) \right. \right. \\ \left. \left. c_{ik}(\xi, \zeta_{\theta\rho}) \rho W_{\theta} W_{\rho} - E_{ij}(\xi, \bar{\xi}_m) \right\} = \\ -p_{ij}^*(\xi, \bar{\xi}_m) \quad ; \quad m = 1, 2, \dots, M \end{aligned} \quad (27)$$

where the first summation is taken over the above mentioned triangular sub-elements, θ and ρ are, respectively, the angular and radial integration variables, $|J|_{\theta\rho}$ and $|G|_{\Delta}$ are the Jacobian introduced by the mapping and subdivision of Γ^j at the integration point $\zeta_{\theta\rho}$ and, W_{θ} and W_{ρ} are the associated weighting factors. The E_{ij} term of eqn (27) is introduced, as before, by the regularization technique, it is now based on a 2-D expansion of c_{ik} into a Taylor series about the singular point.

4.3 Dynamic Applications

In elastodynamic applications (Barra and Telles, 1999), including time harmonic and transient analysis (through inverse numerical transform), the dynamic fundamental solution for 2-D problems (frequency domain) is given in terms of Bessel's function, approximated by polynomial and logarithmic expressions.

The imaginary components of this solution is regular in the frequency domain. The real part of the dynamic fundamental solution when $r \rightarrow 0$ is:

$$Re [P_{11}^*] = \frac{k_0}{r^2} + k_{LRe1} \ln(r) + Re [P_{11}^{Reg}] \quad (28)$$

$$Re [P_{22}^*] = \frac{k_0}{r^2} + k_{LRe2} \ln(r) + Re [P_{22}^{Reg}] \quad (29)$$

where

$$k_0 = \frac{G}{2\pi(1-\nu)} \quad (30)$$

$$k_{LRe1} = -\frac{G\omega^2}{4\pi} \left(\frac{c_p^4 + c_s^4}{c_p^2 c_s^2} \right) \quad (31)$$

$$k_{LRe1} = -\frac{G\omega^2}{4\pi} \left(\frac{3c_p^4 - 4c_p^2 c_s^2 + 3c_s^4}{c_p^4 c_s^2} \right) \quad (32)$$

in which G is the shear modulus, c_p and c_s are compression and shear wave velocities, ω the loading frequency and ν Poisson's ratio. The P_{11}^{Reg} and P_{22}^{Reg} are the regular components of P_{11}^* and P_{22}^* .

If, instead of frequency domain, the Laplace transform domain is adopted, the singularities of the real part of the fundamental solution are still the same. In addition, the imaginary part of the fundamental solution has a logarithmic singularity in the vicinity of ζ_m which is treated in the same fashion as the previous ones:

$$Im [P_{11}^*] = k_{LIm1} \ln(r) + Im [P_{11}^{Reg}] \quad (33)$$

$$Im [P_{22}^*] = k_{LIm2} \ln(r) + Im [P_{22}^{Reg}] \quad (34)$$

Although the singularity terms differ in each approach, the general treatment is the same for both domains. The computation of the correcting term of eqn (17) follows the same pattern, including the logarithmic terms of the real and imaginary parts.

4.4 Plate Bending Applications

In plate bending applications, so far Reissner's plate theory has been implemented. Since the fundamental kernels present singularities of the same order as the 2-D application, the only difference is the number of degrees of freedom which increases to three (one displacement and two rotations) per collocation point (de Figueiredo, 1999).

For Reissner's plate theory, it is customary to represent the stress intensity factors (SIF) associated to the actual moments and shear force. These factors are related to the stress intensity factors calculated at $\pm \frac{h}{2}$ (h is the plate thickness) from the mid surface. For instance, the moment intensity factor " K_I " is expressed as a function of " K_I " stress intensity factor as

$$K_1 = K_I \frac{h^2}{6} \quad (35)$$

5 Examples

In the following examples, continuous elements have been employed throughout the external boundary discretization except for the border crack 3-D in which discontinuity is allowed along the intersection with the crack.

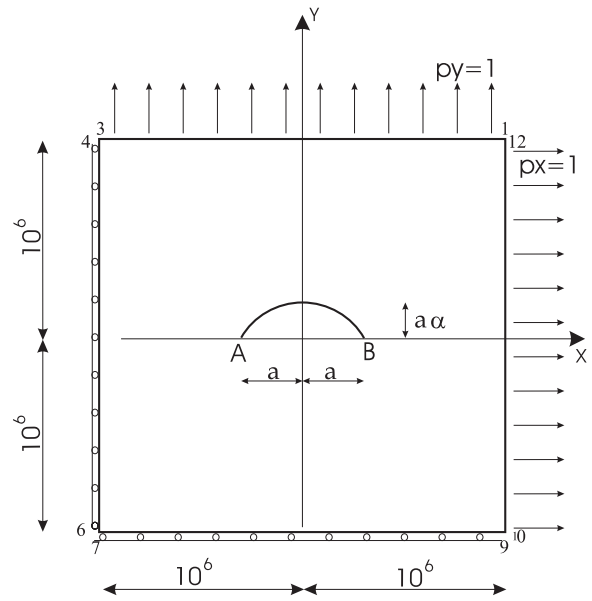


Figure 4 : Parabolic Shape Crack Embedded in an Infinite Remotely Loaded Plate.

5.1 Curved Crack

This example consists of a parabolic shaped crack, depicted in Figure 4, and defined by the expression bellow.

$$y = \frac{\alpha(a^2 - x^2)}{a} \quad (36)$$

The Crack is embedded within a square specimen with remote unit stresses applied in X and Y directions. The numerical model has eight linear elements over the external boundary.

The SIFs were computed from stresses at a point located at $r = 0.004a$ ahead of the crack tip B. The results are shown in Table 1 in comparison to the numerical results given in (Chen, Gross, and Huang, 1991), for $a = 2$ and $\alpha = 0.2$.

Table 1 : Numeric SIF for Crack Problem of Figure 4

SIF	Reference*	NGF	Difference%
K_I	2.3768	2.3928	0.67
K_{II}	-0.4570	-0.4572	0.06

* Chen, Gross, and Huang (1991)

5.2 Infinite Plate in Bending

In this plate bending example Reissner's theory has been applied. The infinite plate was subjected to the bending moments indicated in Figure 5 and Poisson's ratio was 0.3. In this case only matrix S is used to obtain directly the crack opening displacements at the 32 collocation Gauss points. The ones closest to the crack tips have been used to compute the bending

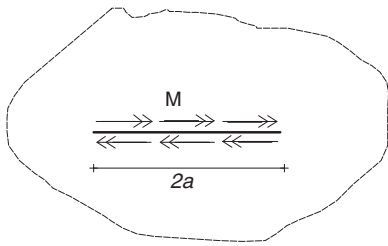


Figure 5 : Bending Moment Applied to Crack Embedded in Infinite Plate

intensity factors. As seen in Table 2, the results compare well with those produced by (Joseph and Erdogan, 1989).

Table 2 : NGF Bending Moment Stress Intensity Factor for Problem of Figure5

$\frac{a}{h}$	$\frac{K_I}{M\sqrt{a}}$	$\frac{K_I}{M\sqrt{a}}^*$	Error%
2.0	0.6832	0.6997	2.36
4.0	0.6630	0.6701	1.06
10.0	0.6567	0.6481	1.33
20.0	0.6656	0.6460	3.03
50.0	0.6559	0.6400	2.48

* Joseph and Erdogan (1989)

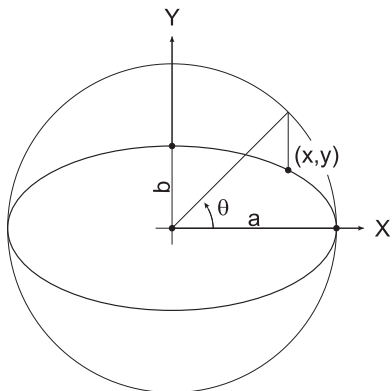


Figure 6 : Plane Elliptical Crack in an Infinite Solid Medium

5.3 Plane Elliptical Crack in a Solid

The problem of a plane elliptical crack, in an infinite medium (Figure 6), under uniform tractions in Z and X directions, can be solved directly with the integral equation (11) (i.e. system of equations (25)). Here, the independent term is equal to the applied internal pressure and there is no need for outer boundary discretization. The geometry of the elliptical crack

has been approximated by a quartic Lagrangean element and the crack opening displacements were calculated at 64 Gauss station positions, corresponding to 8 integration points in each direction. The SIF values have been computed at the second row of Gauss points closest to the crack front. The results are

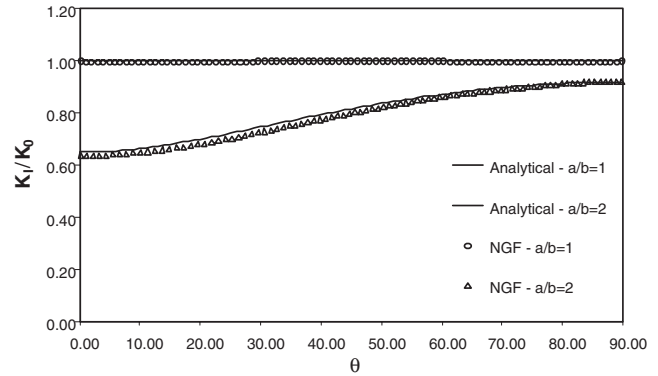


Figure 7 : K_I SIF of a Loaded Elliptical Crack Embedded

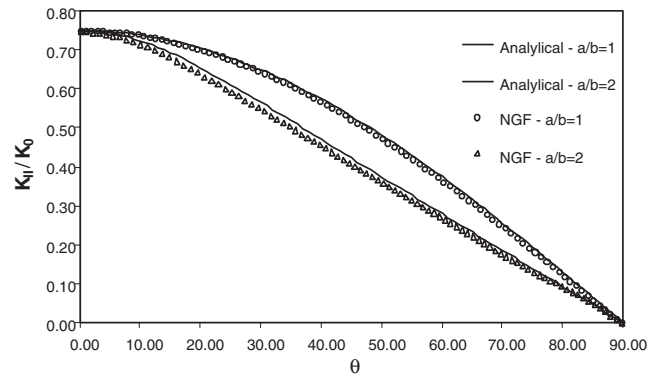


Figure 8 : K_{II} SIF of a Loaded Elliptical Crack Embedded

presented in Figures 7 to 9 for the three SIF computations. The analytical results for mode I are due to (Kassir and Sih, 1967) and for modes II and III are due to (Kassir and Sih, 1966).

5.4 Plane Quarter-circular Border Crack

The problem of a plane quarter-circular crack in a square bar under uniaxial tensile stress, acting in the direction of Z axis, has been discretized by a mesh of 103 quadratic boundary elements in its symmetrical part. The geometry and boundary discretization of the problem are shown in Figure 10. The mode I SIFs have been computed by a least square procedure, using the crack opening displacements weighted by the distance from the crack front. They are presented in Figure 11. An interpolation was introduced in the graphics from $\theta = 42^\circ$ to the corresponding least square result at 45° . The reference results

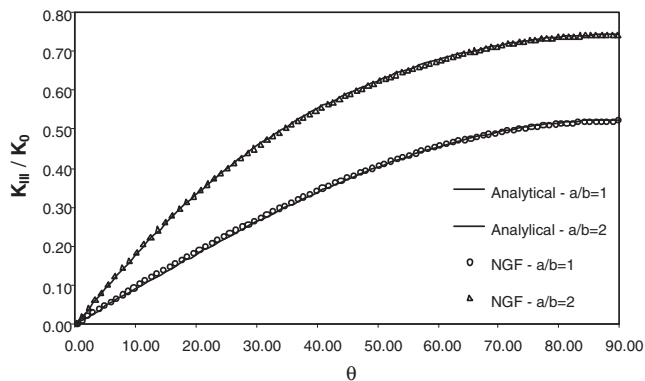


Figure 9 : K_{III} SIF of a Loaded Elliptical Crack Embedded

are due to (Tracey, 1973) and have an accuracy of about 2% (normalized by the SIF of a circular crack of radius a in an infinite medium subject to a remote stress field of intensity σ in the normal direction to the plane of the crack, $K_0 = 2\sigma\sqrt{a/\pi}$).

5.5 Crack in an Infinite Medium Subjected to a Pressure Wave

This example consists of a time harmonic plane pressure wave, acting in the normal direction, upon a flat crack in an infinite medium, ($\nu = 0.25$, plane strain). This problem was previously solved by (Mal, 1970) for plane strains and a wide variety of frequencies. His results permit the comparison presented in Figure (12) where the present NGF solutions are also indicated. The NGF solutions have been computed with only 12 Gauss points for the complete crack. The SIF values were computed using the crack openings and the weighted least square procedure adopted in the previous example.

6 Conclusions

The paper discusses the application of the hyper-singular boundary integral equation to obtain the Green's function solution to general geometry fracture mechanics problems, such as curved multifracture crack simulation, static and harmonic (extended to transient dynamic through inverse numerical transforms), in 2-D, 3-D and plate bending. The implementation presents the same integration difficulties of the mixed (or dual) formulation but leads to smaller system of equations. The accuracy of the solutions illustrates the numerical performance of the approach and its versatility for different applications.

References

Barra, L. P. S.; Telles, J. C. F. (1999): A hyper-singular numerical Green's function generation for BEM applied to dy-

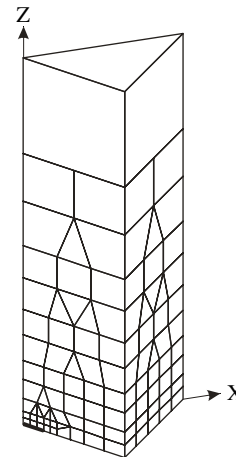


Figure 10 : BEM Mesh With 103 Quadratic Elements and XY Section Plot of The Cracked Bar

namic SIF problems. *Engineering Analysis with Boundary Elements*, vol. 23, pp. 77–87.

Blandford, G. E.; Ingraffea, A. R.; Liggett, J. A. (1981): Two-dimensional stress intensity factor computations using the boundary element method. *International Journal for Numerical Methods in Engineering*, vol. 17, pp. 387–404.

Brebbia, C. A.; Telles, J. C. F.; Wrobel, L. C. (1984): *Boundary Elements Techniques: Theory and Applications in Engineering*. Springer-Verlag.

Castor, G. S.; Telles, J. C. F. (1999): The 3-d BEM implementation of a numerical Green's function for fracture me-

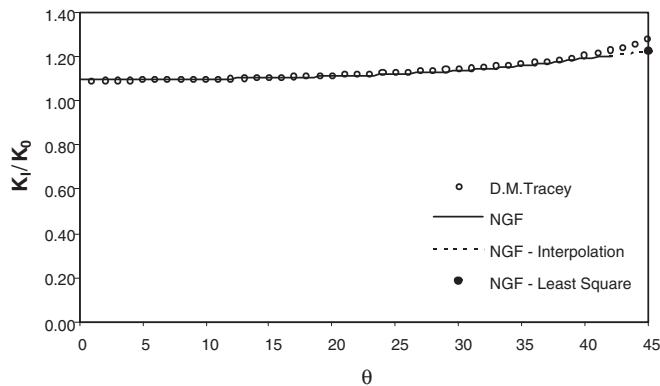


Figure 11 : Mode I SIF for a Plane Quarter-circular Crack in an Square Bar Under Uniaxial Tensile Stress

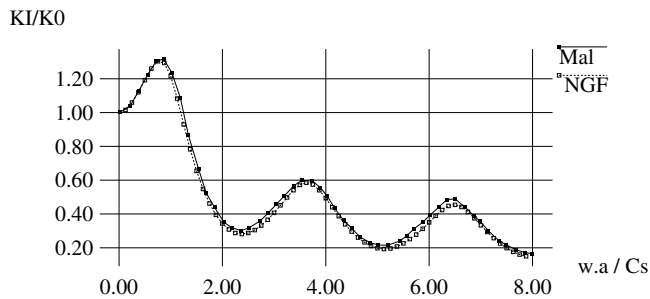


Figure 12 : Dynamic KI for a Crack Embedded in an Infinite Medium.

chanics applications. *International Journal for Numerical Methods in Engineering*, vol. in press.

Chen, Y. Z.; Gross, D.; Huang, Y. J. (1991): Numerical solution of the curved crack problem by means polynomial approximation of the dislocation distribution. *Engineering Fracture Mechanics*, vol. 39, no. 5, pp. 791–797.

Cruse, T. A. (1975): Boundary integral equation method for three dimensional elastic fracture mechanics analysis. Technical Report AFOSR-TR-75-0813, Air Force of Scientific Research, 1975.

de Figueiredo, V. S. (1999): Computation of the numerical Green's function for fracture mechanics problems with Reissner plates. (in portuguese). Master's thesis, COPPE/UFRJ, 1999.

Guimarães, S.; Telles, J. F. C. (1994): On the hyper-singular boundary element formulation for fracture mechanics applications. *Engineering Analysis with Boundary Elements*, vol. 13, pp. 353–363.

Joseph, P. H.; Erdogan, F. (1989): Surface crack problems in plates. *International Journal of Fracture*, vol. 41, pp. 105–131.

Kassir, M. K.; Sih, G. C. (1966): Three-dimensional stress distribution around an elliptical crack under arbitrary loadings. *Journal of Applied Mechanics*, vol. 33, pp. 601–611.

Kassir, M. K.; Sih, G. C. (1967): Griffith's theory of brittle fracture in three dimensions. *International Journal of Engineering Science*, vol. 5, pp. 899–918.

Mal, A. K. (1970): Interaction of elastic waves with a Griffith crack. *International Journal of Engineering Science*, vol. 8, pp. 763–776.

Portela, A.; Aliabadi, M. H.; Rooke, D. P. (1992): Dual boundary element analysis. of cracked plates: Singularity subtraction technique. *International Journal of Fracture*, vol. 55, pp. 17–28.

Silveira, N. P. P.; Guimarães, S.; Telles, J. C. F. (1998): Accurate hypersingular integral computations in the development of numerical Green's function for fracture mechanics. In Sladek, J.; Sladek, V. (1998): editors, *Singular Integrals in Boundary Element Methods*, chapter 6. Computational Mechanics Publication, 1998.

Snyder, M. D.; Cruse, T. A. (1975): Boundary integral equation analysis of cracked anisotropic plates. *International Journal of Fracture*, vol. 11, pp. 315–328.

Telles, J. F. C.; Castor, G. S.; Guimarães, S. (1994): A hypersingular Green's function generation for fracture mechanics problems. In Brebbia, C. A. (1994): editor, *Proc. Boundary Element Method XVI*, pages 443–452, 1994.

Telles, J. F. C.; Castor, G. S.; Guimarães, S. (1995): A numerical Green's function approach for boundary elements applied to fracture mechanics. *International Journal for Numerical Methods in Engineering*, vol. 38, pp. 3259–3274.

Tracey, D. M. (1973): . In *Conference on Finite Element Techniques in Fracture Mechanics*, Stuttgart, Germany, 1973.

